Title

Inherent-state melting and the onset of glassy dynamics in two-dimensional supercooled liquids

Journal

Proceedings of the National Academy of Sciences of the United States of America, 120(14)

ISSN

0027-8424

Authors

Fraggedakis, Dimitrios
Hasyim, Muhammad R
Mandadapu, Kranthi K

Publication Date

2023-04-04

DOI

10.1073/pnas.2209144120

Peer reviewed

PNAS RESEARCH ARTICLE | APPLIED PHYSICAL SCIENCES OPEN ACCESS

Inherent-state melting and the onset of glassy dynamics in two-dimensional supercooled liquids

Dimitrios Fraggedakis[a,1,2], Muhammad R. Hasyim[a,1,2], and Kranthi K. Mandadapu[a,b,2]

Edited by Juan P. Garrahan, University of Nottingham, Nottingham, United Kingdom; received May 26, 2022; accepted February 18, 2023 by Editorial Board Member Mehran Kardar

Below the onset temperature T_o, the equilibrium relaxation time of most glass-forming liquids exhibits glassy dynamics characterized by a super-Arrhenius temperature dependence. In this supercooled regime, the relaxation dynamics also proceeds through localized elastic excitations corresponding to hopping events between inherent states, i.e., potential-energy-minimizing configurations of the liquid. Despite its importance in distinguishing the supercooled regime from the high-temperature regime, the microscopic origin of T_o is not yet known. Here, we construct a theory for the onset temperature in two dimensions and find that an inherent-state melting transition, described by the binding–unbinding transition of dipolar elastic excitations, delineates the supercooled regime from the high-temperature regime. The corresponding melting transition temperature is in good agreement with the onset temperature found in various two-dimensional (2D) atomistic models of glass formers and an experimental binary colloidal system confined to a water–air interface. Additionally, we find the predictions for the renormalized elastic moduli to agree with the experimentally observed values for the latter 2D colloidal system. We further discuss the predictions of our theory on the displacement and density correlations at supercooled conditions, which are consistent with observations of the Mermin–Wagner fluctuations in experiments and molecular simulations.

two-dimensional glassy dynamics | Kosterlitz–Thouless transition | excitations | geometric charges | onset of glassy dynamics

The dynamics of glass-forming liquids slows down significantly below an onset temperature T_o (1–4), as seen in the cross-over from Arrhenius ($T > T_o$) to super-Arrhenius ($T < T_o$) growth of the equilibrium relaxation time τ_{eq} (Fig. 1*A*). The cross-over is also observed in the mean squared displacement (MSD) (5), as shown in Fig. 1*B*. Above T_o, the MSD is characterized only by the ballistic and diffusive regimes (6). For $T < T_o$, however, a new intermediate (glassy) regime appears where the MSD exhibits a plateau-like shape that is reminiscent of solids (7, 8). In two dimensions (2D), this solid-like behavior manifests as Mermin–Wagner fluctuations (9, 10), which are long-wavelength fluctuations typically associated with 2D elastic solids. Recent experiments in 2D colloidal systems and molecular simulations have shown that such fluctuations affect the finite-size scaling of the MSD and density autocorrelations (11–15).

The supercooled liquid, i.e., liquid below T_o, is further characterized by dynamical heterogeneity (16), where particles initially move in sparse "mobile" regions that spread over time (17, 18). These initial mobile regions are spatially localized and can be classified as excitations (17, 19) that drive particle hopping dynamics, while the rest of the system vibrates around its initial state (Fig. 1 *B*, *Inset*). The excitations correspond to hopping events between neighboring inherent-state (IS) configurations, which are the energy-minimized configurations in the potential energy landscape (20). This excitation-based perspective is central to the dynamical facilitation (DF) theory (21), one of the theories describing the super-Arrhenius relaxation behavior. In DF theory, dynamical heterogeneity is understood in terms of excitations facilitating the formation and relaxation of nearby excitations in a hierarchical manner (17, 22). For $T > T_o$, however, particle motion occurs with little to no dynamical heterogeneity (Fig. 1 *B*, *Inset*), suggesting a different relaxation mechanism.

While various theories (21, 23–26) have attempted to explain the dynamics of liquids below the onset temperature T_o, none, so far, have identified the physical nature of this cross-over, thereby determining the value of T_o itself. Taken together, the qualitative differences on the dynamics above and below T_o raise the following questions: i) What is the microscopic origin of T_o that distinguishes normal liquids from supercooled liquids?

Significance

The dynamics of glass formers exhibit dramatic slowdown below an onset temperature that delineates the high-temperature and supercooled regimes. For two-dimensional (2D) glass formers, we propose that the onset temperature is described by a Kosterlitz–Thouless transition driven by the elastic excitations underlying the relaxation mechanism for glassy dynamics. Analogous to dislocation-mediated melting in 2D solids, the excitations exist as a bound dipole–dipole state in the supercooled regime and as free dipoles above the onset temperature. The Kosterlitz–Thouless scenario explains the elastic behavior of 2D supercooled liquids at intermediate timescales and thus, the Mermin–Wagner fluctuations observed in experiments and simulations of 2D glass formers. The present work reveals the exotic nature of 2D glass formers relevant to systems under extreme confinement.

The authors declare no competing interest.

This article is a PNAS Direct Submission. J.P.G. is a guest editor invited by the Editorial Board.

[1]D.F. and M.R.H. contributed equally to this work.

[2]To whom correspondence may be addressed. Email: dimfraged@gmail.com, muhammad_hasyim@berkeley.edu, kranthi@berkeley.edu.

This article contains supporting information online at http://www.pnas.org/lookup/suppl/doi:10.1073/pnas.2209144120/-/DCSupplemental.

Published March 31, 2023.

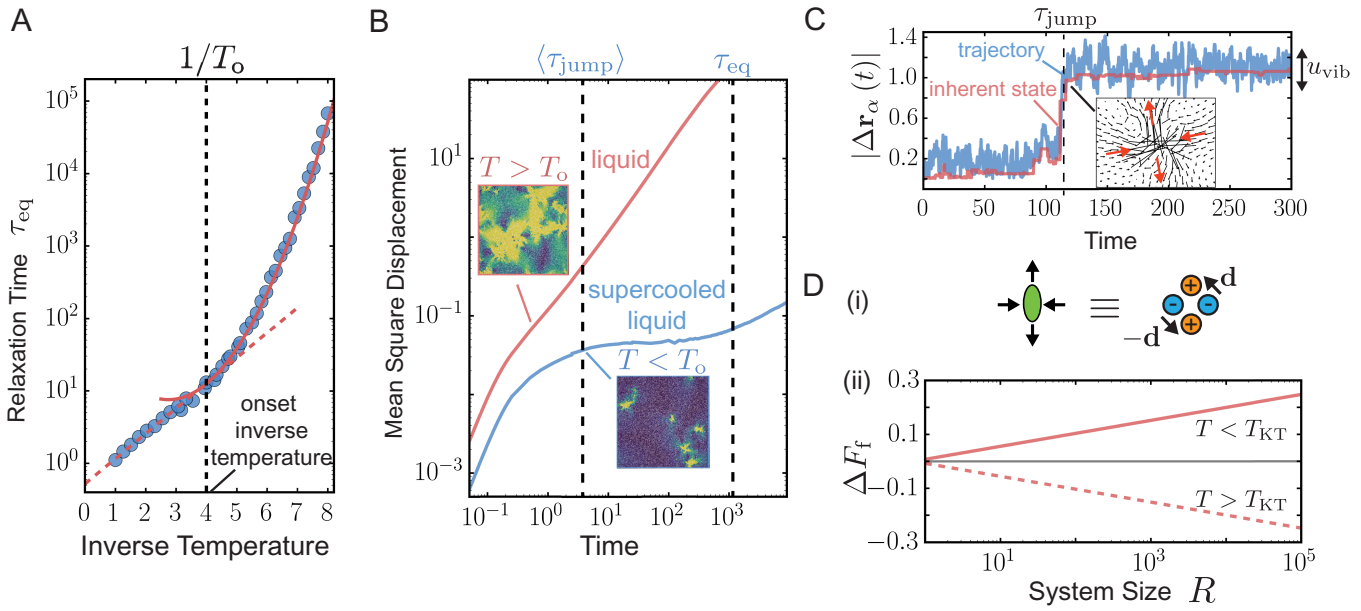

Fig. 1. (*A*) Equilibrium relaxation time τ_{eq} as a function of the inverse temperature. For $T > T_o$, τ_{eq} follows the classical Arrhenius behavior, while for $T < T_o$, it has a super-Arrhenius temperature dependence. (*B*) Mean squared displacement vs. time for $T > T_o$ (red line) and $T < T_o$ (blue line). *Inset*: Inherent-state (IS) particle displacement magnitude field showing the mobile regions at two different temperatures. At $T < T_o$, there exists an intermediate regime where only few localized mobile regions are observed. At $T > T_o$, the system enters the diffusive regime immediately after the ballistic one, with mobile regions spanning the entire system. Vertical dashed lines correspond to jump time $\langle\tau_{jump}\rangle$ and relaxation time τ_{eq} under supercooled conditions. (*C*) A particle trajectory (blue line) and its corresponding IS trajectory (red line) at $t = \tau_{jump}$ when an excitation occurs. *Inset*: The corresponding IS displacement vector field showing the pure-shear deformation induced by the excitation. (*D*, *i*) Correspondence of a pure-shear transformation, shown in *Inset* of (*C*), with two bound elastic "dipoles" of net zero dipole moment. (*D*, *ii*) Free energy of formation, ΔF_f, of dipolar elastic excitations vs. system size R. For $T < T_{KT}$ (continuous red line), the formation of free dipoles is not energetically favorable, indicating the formation of bound dipoles at these temperatures instead, as in (*D*, *i*). For $T > T_{KT}$ (dashed red line), entropy changes the sign of ΔF_f allowing the formation of free dipoles. In all cases, the parameters used correspond to the Poly-(12,0) model glass former (*SI Appendix*, section 5.4).

ii) Does T_o signal a change in the relaxation mechanism between these two regimes? And iii) how is T_o connected to the solid-like nature of supercooled liquids at intermediate timescales?

In this work, we address these questions related to 2D supercooled liquids by constructing a theory where the origin of T_o lies within the statistical mechanics of excitation events. To demonstrate this, we focus on the time evolution of particles within the intermediate timescales of

$$\tau_{vib}(T) \ll t \sim \langle\tau_{jump}(T)\rangle \ll \tau_{eq}(T), \qquad [1]$$

where $\tau_{vib}(T)$ is the characteristic vibrational timescale, and $\langle\tau_{jump}(T)\rangle$ corresponds to the average time needed for a particle to hop to its next position; Fig. 1*C*. The particle dynamics at these timescales are characterized by the instantaneous IS positions $\mathbf{R}^\alpha(t)$. The IS trajectory coarse-grains the vibrational motion, and hopping in particle motions is reflected as jumps in the IS positions at $t = \tau_{jump}$ (27). Within the perspective of DF theory (17, 21), recent work (19) indicates that jumps between inherent states correspond to excitation events, which induce localized pure-shear deformations (19, 28) (Fig. 1 *C*, *Inset*). One of the main ideas of the present work is that, analogous to electrostatics, an excitation in 2D can be modeled as two bound elastic "dipoles" (29, 30); Fig. 1 *D*, *i* and *SI Appendix*, section 2.2. This physical picture of excitations is distinct from other works in amorphous media, which utilize the notion of quasi-localized excitations (31–33). If dipoles are considered to be the fundamental units of excitations, then an energy–entropy argument for their formation hints toward a transition temperature T_{KT} (Fig. 1 *D*, *ii* and *SI Appendix*, section 3.1) that governs the unbinding of localized excitations into free dipoles and thus leads to a change in relaxation mechanism. Furthermore, the binding–unbinding transition is analogous to the one described by the Kosterlitz–Thouless–Halperin–Nelson–Young (KTHNY) theory (34–39) of dislocation-mediated melting. This, in turn, provides an alternative picture of the transition in terms of inherent states "melting" into a high-temperature fluid, with the transition temperature being the onset temperature.

Theory

To establish a thermodynamic framework for understanding the onset temperature T_o via excitation events, we begin by constructing an isoconfigurational ensemble (40) that corresponds to jumps between a given IS and its neighboring states in the potential energy landscape. Conceptually, such a construction is understood through Fig. 1*C*, where a single trajectory provides one sample realization of a single jump that takes the system from its initial IS configuration $\{\mathbf{R}_0^\alpha\}$ to one of its neighboring ISs at $t = \tau_{jump}$, where τ_{jump} is a random variable (*SI Appendix*, section 1.1). The isoconfigurational ensemble can then be built by initiating multiple trajectories from $\{\mathbf{R}_0^\alpha\}$ that eventually visit all possible neighboring ISs (Fig. 2 *A*, *i*). The set of all neighboring ISs of $\{\mathbf{R}_0^\alpha\}$, $\mathcal{B}(\{\mathbf{R}_0\})$, sampled by the isoconfigurational ensemble, forms a basis for an ensemble of excitation configurations. Given the energy landscape complexity, not all neighboring ISs are visited with the same frequency. Under the main assumptions of transition state theory (41, 42), i.e., equilibrium between the reactant (the initial inherent state) and transition states as well as no recrossing at the transition state, we can define the conditional probability to visit a neighboring IS as $p_{iso} = e^{-\beta\Delta U^\ddagger}/Q_{iso}(\{\mathbf{R}_0^\alpha\})$ (Fig. 2 *A*, *ii* and *SI Appendix*, section 1.1). Here, $\Delta U^\ddagger$ is the potential energy

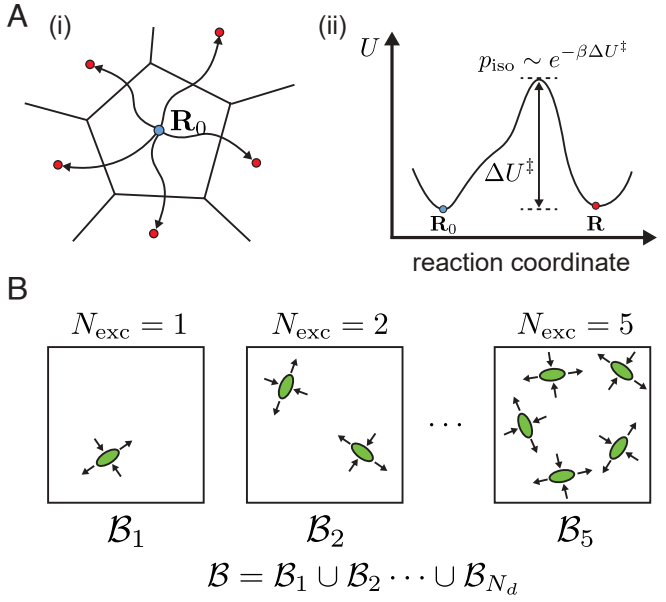

Fig. 2. (*A*)–(*i*) Illustration of inherent-state (IS) jumps in configuration space obtained using the isoconfigurational ensemble. (*A*)–(*ii*) Potential energy landscape that defines the conditional probability, $p_{\rm iso}$, for visiting state $\mathbf{R}$ starting from $\mathbf{R}_0$ in terms of the transition state energy barrier $\Delta U^\ddagger$. (*B*) Schematic of the subsets of the set of all possible nearest-neighboring inherent states $\mathcal{B}$ organized in terms of the excitation number. In this schematic, excitations lead to localized pure-shear transformations in the medium, consistent with refs. 19 and 28.

barrier, $\beta = 1/k_{\rm B}T$ with $k_{\rm B}$ being the Boltzmann constant, and $Q_{\rm iso}(\{\mathbf{R}_0^\alpha\}) = \sum_{\{\mathbf{R}^\alpha\}\in\mathcal{B}(\{\mathbf{R}_0^\alpha\})} e^{-\beta\Delta U^\ddagger}$ is the normalization constant. Note that $Q_{\rm iso}(\{\mathbf{R}_0^\alpha\})$ defines the isoconfigurational partition function that can be used to study the statistics of IS jumps from all possible initial ISs upon averaging it over the IS ensemble (*SI Appendix*, sections 1.1 and 1.2). This procedure leads to the IS-averaged partition function

$$\bar{Q}_{\rm iso} = \left\langle \sum_{\{\mathbf{R}^\alpha\}\in\mathcal{B}(\{\mathbf{R}_0^\alpha\})} e^{-\beta\Delta U^\ddagger} \right\rangle_{\rm IS}, \qquad [2]$$

where $\bar{Q}_{\rm iso} = \langle Q_{\rm iso}(\{\mathbf{R}_0^\alpha\})\rangle_{\rm IS}$, and $\langle\ldots\rangle_{\rm IS}$ is an ensemble average over all possible ISs.

An IS jump can lead to the formation of multiple excitations in space. Thus, we can express $\mathcal{B}$ as a union of subsets that contain $N_{\rm exc}$ excitations, $\mathcal{B} = \bigcup_{N_{\rm exc}=1}^{N_{\rm d}} \mathcal{B}_{N_{\rm exc}}$, where $N_{\rm d}$ is the maximum number of excitations bounded by the total number of particles (Fig. 2*B*). This representation allows us to consider excitations as quasi-particles described by their positions $\{\mathbf{q}^\mu\}$ and internal degrees of freedom $\{\mathbf{s}^\mu\}$. As a result, we derive from Eq. **2** a grand canonical partition function for a thermodynamic ensemble of excitations (*SI Appendix*, section 1.2).

$$\bar{\Xi}_{\rm exc} = 1 + \bar{Q}_{\rm iso} = \sum_{N_{\rm exc}=0}^{N_{\rm d}} Z_{N_{\rm exc}} \tilde{y}^{N_{\rm exc}} \qquad [3a]$$

$$Z_{N_{\rm exc}} = \frac{1}{N_{\rm exc}!} \int \prod_{\mu=1}^{N_{\rm exc}} \frac{{\rm d}^d\mathbf{q}^\mu \, {\rm d}^{d_{\rm int}}\mathbf{s}^\mu}{(a_{\rm exc})^{dN_{\rm exc}}} e^{-\tilde{\mathcal{H}}}, \qquad [3b]$$

where $a_{\rm exc}$ is the size of excitations, $\tilde{y} = e^{-\tilde{E}_{\rm c}}$ is the fugacity that defines the concentration of excitations via their dimensionless self-energy $\tilde{E}_{\rm c} = \beta\bar{E}_{\rm c}$, and $\tilde{\mathcal{H}} = \sum_{\langle\mu,\gamma\rangle} \tilde{v}^{\mu\gamma}$, with $\tilde{v}^{\mu\gamma} = \beta\bar{v}^{\mu\gamma}$, is the dimensionless total interaction energy of pairs of excitations.

Eq. **3a** allows us to find the equilibrium concentration of noninteracting excitations as $c_{\rm eq}(T) \sim e^{-\beta\bar{E}_{\rm c}}$ (*SI Appendix*, section 1.3). The same Arrhenius form of $c_{\rm eq}(T)$ is found in kinetically constrained models (43, 44), as used by the DF theory, to model hierarchical relaxation caused by excitations (21). It is also consistent with the rate of particle-hopping events $c_\sigma(T)$, which is a proxy for $c_{\rm eq}(T)$ in molecular simulations for the DF theory since $c_\sigma(T)$ is empirically observed to be of the Arrhenius form (17, 19).

The framework of geometric charges (29, 30) provides us a way to describe the formation of excitations in glass formers. Geometric monopoles, dipoles, quadrupoles, or higher-order multipoles are therefore candidates for describing elementary excitations*. To determine which geometric charges are thermodynamically admissible, we resort to their free energy of formation in an elastic medium, $\Delta F_{\rm f}$ (*SI Appendix*, section 3.1). For monopoles with charge m, we find $\Delta F_{\rm f}^{\rm mnpl} \sim mR^2 \geq 0$ for all R and T, where R is the size of the system. We therefore conclude that geometric monopoles are not thermodynamically favorable. For dipoles with dipole moment magnitude $d_{\rm c}$, the free energy is $\Delta F_{\rm f}^{\rm dpl} \sim \left(\frac{d_{\rm c}^2 Y}{8\pi} - 2k_{\rm B}T\right)\ln R$, where Y is Young's modulus; Fig. 1 *D*, *ii*. When $k_{\rm B}T < d_{\rm c}^2 Y/16\pi$, we find $\Delta F^{\rm dpl} > 0$ which implies that spontaneous formation of single dipoles is not favored. For $k_{\rm B}T > d_{\rm c}^2 Y/16\pi$, however, the free energy becomes negative, $\Delta F_{\rm f}^{\rm dpl} < 0$, and free dipole formation is preferred. This qualitative change on the sign of $\Delta F_{\rm f}^{\rm dpl}$ at $T_{\rm c} = d_{\rm c}^2 Y/16\pi k_{\rm B}$ hints toward a binding-unbinding transition analogous to the KTHNY theory. For quadrupoles, $\Delta F_{\rm f}^{\rm qdpl} \sim -\ln R$ which leads to $\Delta F_{\rm f}^{\rm qdpl} < 0$ for large R, and thus, their formation is thermodynamically admissible for all T. Quadrupoles consist of two bound dipoles in the limit of infinitesimal separation (Fig. 1 *D*, *i*), and this motivates us to investigate the binding-unbinding transition through similar free-energy arguments. In particular, we find the temperature for which two free dipoles are preferred when compared to the bound dipole-pair state to be $T_{\rm c}' = d_{\rm c}^2 Y/8\pi k_{\rm B}$ (*SI Appendix*, section 3.1). The observation that this transition temperature differs from that of the free-energy argument of a single dipole is a result of neglecting interactions between the two dipoles. Thus, a more complete picture that involves a grand canonical ensemble of interacting dipolar excitations is required to understand the binding-unbinding transition, which we proceed to analyze.

An ensemble of interacting dipoles is described by their (dimensionless) self-energy $\tilde{E}_{\rm c}$ and interaction $\tilde{v}^{\mu\gamma}$, which can be derived following the use of geometric charge and dipole moment conservation laws (*SI Appendix*, sections 2.3 and 2.4). This yields,

$$\tilde{E}_{\rm c} = \frac{\tilde{Y}^{\rm IS}}{8\pi}(\tilde{C}+1), \qquad [4a]$$

$$\tilde{v}^{\mu\gamma} = \frac{\tilde{Y}^{\rm IS}}{4\pi}\left(\tilde{d}_i^\mu \tilde{d}_i^\gamma \left(1 - \ln\frac{q^{\mu\gamma}}{a_{\rm dpl}}\right) - \frac{\tilde{d}_i^\mu q_i^{\mu\gamma} \tilde{d}_j^\gamma q_j^{\mu\gamma}}{(q^{\mu\gamma})^2}\right), \qquad [4b]$$

SI Appendix, section 2.2 for a discussion of how geometric charges can be mapped to classical defects in crystalline solids, such as disclinations, dislocations, and point defects.

where $\tilde{Y}^{\mathrm{IS}} = \beta d_c^2 Y^{\mathrm{IS}}$, with Y^{IS} being the IS Young's modulus, $q_i^{\mu\gamma} = q_i^{\mu} - q_i^{\gamma}$, a_{dpl} is the dipole size, $\tilde{d}_i^{\mu} = d_i^{\mu}/d_c$ is the dimensionless dipole moment vector; *SI Appendix*, sections 3.2 and 3.4 for the derivation of Eq. **4a** and **b**. We determine the dipole moment magnitude d_c and the constant $\tilde{C}$ following the mapping between bound geometric dipoles and localized pure-shear excitations (*SI Appendix*, section 3.3), which were modeled previously via a force-dipole formalism (19). This mapping ensures the equivalency between the average energy barrier and the spatial stress distributions corresponding to excitations and yields (*SI Appendix*, section 3.3)

$$d_c = \frac{2\pi R_{\mathrm{exc}}\epsilon_c}{\nu^{\mathrm{IS}}+1}, \quad \tilde{C} = \frac{3+\nu^{\mathrm{IS}}}{4}, \qquad [5]$$

where $R_{\mathrm{exc}} = a_{\mathrm{dpl}}/\sqrt{2}$, and the eigenstrain, ϵ_c is determined from the knowledge of local structure; equations 34–35 in ref. 19.

Analogous to the KTHNY theory, we now study the dipole binding-unbinding transition via its impact on the elastic response of an IS in the presence of excitations. The dimensionless stiffness tensor $\tilde{C}^{\mathrm{R}}_{ijkl}$ governing this response can be written using any combination of two elastic constants due to isotropy of glass formers. Choosing Young's (Y^{R}) and shear (G^{R}) moduli, a static linear response theory yields (*SI Appendix*, sections 4.1 and 4.2)

$$\frac{1}{\tilde{G}^{\mathrm{R}}} = \frac{1}{\tilde{G}^{\mathrm{IS}}} + \frac{A_0}{d_c^2}\left(\langle\hat{\epsilon}^{\mathrm{e}}_{ij}\hat{\epsilon}^{\mathrm{e}}_{ij}\rangle - \frac{1}{2}\langle\hat{\epsilon}^{\mathrm{e}}_{ii}\hat{\epsilon}^{\mathrm{e}}_{kk}\rangle\right), \qquad [6a]$$

$$\frac{1}{\tilde{Y}^{\mathrm{R}}} = \frac{1}{\tilde{Y}^{\mathrm{IS}}} + \frac{A_0}{4d_c^2}\left(\langle\hat{\epsilon}^{\mathrm{e}}_{ij}\hat{\epsilon}^{\mathrm{e}}_{ij}\rangle + \frac{1}{2}\langle\hat{\epsilon}^{\mathrm{e}}_{ii}\hat{\epsilon}^{\mathrm{e}}_{kk}\rangle\right), \qquad [6b]$$

where A_0 is the area of the medium, $\hat{\epsilon}^{\mathrm{e}}_{ij}$ is the area-averaged elastic strain due to the presence of geometric dipoles, and $\langle\ldots\rangle$ denotes the grand canonical ensemble average. The transition is then determined by locating the temperature above which $\tilde{G}^{\mathrm{R}} = 0$ and $\tilde{Y}^{\mathrm{R}} = 0$ corresponding to the loss of elastic moduli as a result of the dipole-mediated melting of ISs.

Since the fugacity $\tilde{y}$ is small (*SI Appendix*, Table S.1 and section 5.1), Eq. **6a** and **b** can be evaluated by a fugacity series expansion around $\tilde{y} = 0$; such a procedure, however, leads to divergent expressions near the unbinding/melting transition. This situation can be remedied via the renormalization group (RG) procedure (38, 45, 46), which uses the initial fugacity expansion to obtain the following set of RG equations for the fugacity, Young's and shear moduli (*SI Appendix*, sections 5.1 and 5.2)

$$\frac{d\tilde{y}}{d\ell} = \left(2 - \frac{\tilde{Y}}{8\pi}\right)\tilde{y} + 2\pi\tilde{y}^2 e^{\frac{\tilde{Y}}{16\pi}} I_0\left(\frac{\tilde{Y}}{8\pi}\right), \qquad [7a]$$

$$\frac{d\tilde{Y}^{-1}}{d\ell} = \frac{\pi^2}{4}\tilde{y}^2 e^{\frac{\tilde{Y}}{8\pi}}\left(2I_0\left(\frac{\tilde{Y}}{8\pi}\right) - I_1\left(\frac{\tilde{Y}}{8\pi}\right)\right), \qquad [7b]$$

$$\frac{d\tilde{G}^{-1}}{d\ell} = \pi^2\tilde{y}^2 e^{\frac{\tilde{Y}}{8\pi}} I_0\left(\frac{\tilde{Y}}{8\pi}\right), \qquad [7c]$$

where $I_n(x)$ is the nth order modified Bessel function of the first kind, and ℓ is associated with the logarithm of a lengthscale. The renormalized elastic moduli are then obtained by integrating Eq. **7a–c** to the large-ℓ limit with initial conditions given by $\tilde{G}(0) = \tilde{G}^{\mathrm{IS}}$, $\tilde{Y}(0) = \tilde{Y}^{\mathrm{IS}}$, and $\tilde{y}(0) = e^{-\tilde{E}_c}$, where $\tilde{E}_c$ is provided by Eq. **4a**.

Eq. **7a–c** are very similar to the RG equations of the KTHNY theory (38, 39), with the exception of the π^2 factor in Eq. **7a** and **b** that replaces the usual factor of 3π. This difference stems from the continuous orientability of dipoles in amorphous media in contrast to crystalline solids where only discrete values are allowed. Despite this, the difference yields only a minor change in the critical exponent describing the vanishing elastic moduli near T_{KT} (*SI Appendix*, section 5.3). Nevertheless, from the RG flow equations, we observe that working only with $\tilde{Y}$ and $\tilde{y}$ is sufficient to understand the melting transition, given all flow equations depend exclusively on these two variables.

Results

Theoretical Analysis and Predictions. We start by analyzing Eq. **7a** and **b** in terms of their fixed points $(\tilde{y}^*, \tilde{Y}^*)$, where we find the RG flow equations to be stationary for $\tilde{y}^* = 0$ and any value of $\tilde{Y}^*$ (*SI Appendix*, section 5.3). This behavior is seen in Fig. 3*A*, where we show the phase portrait for $\tilde{y}$ and $8\pi/\tilde{Y}$. We observe that for any initial point starting within the region below the separatrix (green dashed line), the flow converges toward the locus of $\tilde{y}^* = 0$ and $\tilde{Y}^* \neq 0$ (red line), indicating the existence of a solid phase where a supercooled liquid behaves elastically at intermediate timescales. For $\tilde{Y}^* \leq 16\pi$, however, the family of fixed points becomes unstable to any infinitesimal perturbations around $\tilde{y}^* = 0$ (*SI Appendix*, section 5.3), indicating the fluid phase. This implies that the separatrix controls the location of the melting point. Thus, the melting temperature T_{KT} is obtained by finding the initial conditions $(\tilde{Y}^{\mathrm{IS}}(T_{\mathrm{KT}}), \tilde{y}(T_{\mathrm{KT}}))$ that lie on the separatrix so that the RG flow converges to the fixed point $(\tilde{Y}^{\mathrm{R}}, \tilde{y}_{\mathrm{R}}) = (16\pi, 0)$. In Fig. 3*A*, we show in red dashed line a set of initial conditions that terminates at the separatrix.

To validate our hypothesis that T_{KT} corresponds to the onset temperature for glassy dynamics T_o, we test the theory on seven models of glass-forming liquids (*SI Appendix*, section 5.4). Here, we take the perspective of DF theory for estimating T_o, which is done by fitting the parabolic law, $\ln\tau_{\mathrm{eq}} \sim J^2(\beta - \beta_o)^2$, to the relaxation time data (3, 4), where $\beta_o = 1/k_B T_o$, and J is an effective energy scale. Estimation of T_o can also be done via computation of the particle-hopping rate $c_\sigma(T)$ from coarse-grained particle trajectories. This quantity is empirically observed to be Arrhenius at short-intermediate timescales and $T \leq T_o$, i.e., $c_\sigma(T) \sim e^{-J_\sigma(\beta-\beta_o)}$ with $J_\sigma \sim J$, indicating the onset of activated dynamics (17, 19). Both estimates have been shown to agree with each other (17, 19) and delineate the supercooled and high-temperature regimes. In this work, we choose the parabolic law fitting for estimating T_o. We evaluate the IS melting transition in two ways: 1) the approximate estimate $T^{\mathrm{app}}_{\mathrm{KT}} = d_c^2 Y^{\mathrm{IS}}/16\pi k_B$ that assumes $\tilde{y} = 0$, and thus, no renormalization occurs on Young's modulus, and 2) the true estimate T_{KT} based on the intersection of the separatrix with the curve of initial conditions for different models, where numerical integration of Eq. **7a** and **b** is performed (*SI Appendix*, section 5.4).

Table 1 summarizes the results of our theory compared to the estimated T_o for these models. In all cases, the true estimate of the melting temperature T_{KT} based on RG procedure is in reasonable agreement with the observed onset temperature. On the contrary, $T^{\mathrm{app}}_{\mathrm{KT}}$ typically overestimates the transition point, which may be attributed to ignoring the renormalization of Young's modulus. Fig. 3*B* shows the bare $\tilde{Y}^{\mathrm{IS}}$ and renormalized

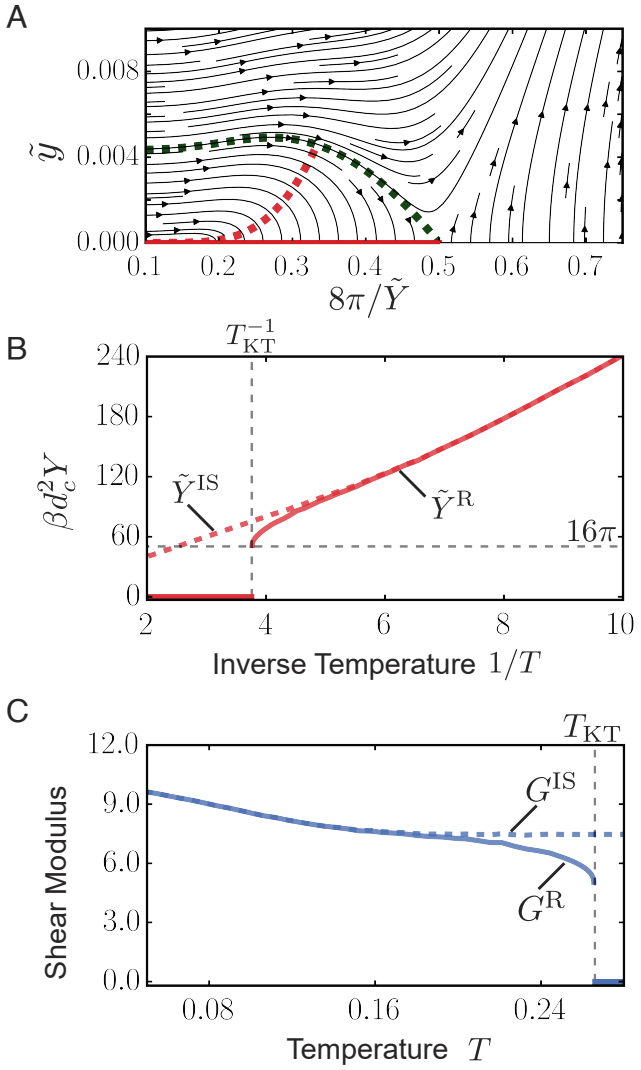

Fig. 3. (*A*) Phase-space portrait of the RG equations in Eq. **7a** and **b**. Horizontal red line corresponds to the locus of fixed points terminating at $\tilde{Y} = 16\pi$. The separatrix (green dashed line), distinguishes the supercooled regime from the high-temperature regime. Red dashed line is the possible initial conditions for the RG flow. (*B*) The renormalized (bold line) and bare (dashed line) values of the normalized Young's $\tilde{Y} = \beta d_c^2 Y$ modulus vs. inverse temperature $1/T$. At $T = T_{\rm KT}$, $\tilde{Y}$ vanishes discontinuously after attaining the universal value of 16π (37). (*C*) Bare, $G^{\rm IS}$, and renormalized, $G^{\rm R}$, shear modulus vs. temperature. As T is increased, $G^{\rm IS}$ shows a linear dependence in T until a temperature where $G^{\rm IS}$ reaches a plateau. Meanwhile, $G^{\rm R}$ moves away from $G^{\rm IS}$ as T is increased and drops to zero at $T = T_{\rm KT}$, where the supercooled liquid phase loses its rigidity. In (*A–C*) the parameters used correspond to the Poly-(12,0) model glass former.

$\tilde{Y}^{\rm R}$ Young's modulus as a function of temperature. We observe that $\tilde{Y}^{\rm R} < \tilde{Y}^{\rm IS}$ due to a softening effect caused by excitations on the elastic stiffness of the inherent states. At $T = T_{\rm KT}$, $\tilde{Y}^{\rm R}$ vanishes discontinuously once the universal value of 16π is reached. For $\tilde{t} = 1 - T/T_{\rm KT} \ll 1$, using perturbative analysis, we can derive a power law form for the decay of Young's modulus as $\tilde{Y}^{\rm R}(T) = 16\pi(1 + \bar{C}\ \tilde{t}^{\bar{\nu}_{\rm KT}})$, where $\bar{\nu}_{\rm KT} \simeq 0.372$, and $\bar{C}$ is a nonuniversal constant (*SI Appendix*, section 5.3). This discontinuous behavior also extends to the renormalized shear modulus $G^{\rm R}$, as shown in Fig. 3*C*, with $G^{\rm R} \to G^{\rm IS}$ as $T \to 0$.

Our theory also provides a way to study displacement and density correlations of supercooled liquids at intermediate timescales. In particular, our theory suggests that supercooled liquids behave as solids at timescales $t \simeq \langle \tau_{\rm jump} \rangle$. We can thus assume that their elastic response at intermediate timescales can be described using a Gaussian field theory, with the elastic constants being the renormalized ones obtained from the RG flow equations. This idea is linked to the nature of the RG flow which coarse-grains a solid with excitations into a "softer" solid without excitations. The coarse-graining lengthscale is set by ξ^* and represents the average size of bound dipoles above which the Gaussian field theory is valid. The value of ξ^* increases with temperature and diverges near the critical point $T_{\rm KT}$, where melting takes place. For temperatures deep in the supercooled regime, $\xi^* \sim \mathcal{O}(a_{\rm dpl}) \sim \mathcal{O}(\sigma_{\rm d})$, where $\sigma_{\rm d}$ is the particle diameter (*SI Appendix*, section 5.5) corresponding to tightly bound elastic dipoles. To understand the behavior of the mean-squared displacement and density–density correlations in renormalized 2D linear elastic solids, we use ξ^* and the system size R as the lower and upper cutoff lengths, respectively, in the field theory. Following such an approach, we find the MSD to be (*SI Appendix*, section 5.5)

$$\left\langle |\mathbf{u}(\langle \tau_{\rm jump} \rangle)|^2 \right\rangle \simeq k_{\rm B} T \frac{(3 - \nu^{\rm R})(1 + \nu^{\rm R})}{2\pi Y^{\rm R}} \ln \frac{R}{\xi^*}. \qquad [8]$$

Eq. **8** is a signature of the Mermin–Wagner fluctuations in 2D solids and is consistent with observations from experiments and computer simulations of glass formers (11–15). In Fig. 4*A*, we plot the logarithmic scaling, as predicted for the Poly-(12,0) model glass former for two different temperatures.

The signatures of Mermin–Wagner fluctuations are also reflected in the self-part of the intermediate scattering function $F_s(k, t)$, where the theory suggests (*SI Appendix*, section 5.5)

$$F_s(k, \langle \tau_{\rm jump} \rangle) \simeq \left(\frac{R}{\xi^*} \right)^{-\frac{\sigma(k,T)}{2}}, \qquad [9a]$$

$$\sigma(k, T) = k_{\rm B} T \frac{k^2 \left(3 - \nu^{\rm R}\right)\left(1 + \nu^{\rm R}\right)}{4\pi Y^{\rm R}}, \qquad [9b]$$

which is valid for wavenumber $k \in [0, 2\pi/\xi^*]$. Since $\xi^* \sim \mathcal{O}(\sigma_{\rm d})$ as $T \to 0$, Eq. **9a** becomes valid at lengthscales in which we typically measure relaxation dynamics, e.g., $k = 2\pi/\sigma_{\rm d}$. Thus, relaxation, as measured by $F_s(k, t)$, proceeds faster with

Table 1. Comparison of the onset temperature $T_{\rm o}$, obtained through parabolic law fitting of $\tau_{\rm eq}$ (3, 4), with the predicted transition temperature $T_{\rm KT}$ for the binding-unbinding transition of dipolar elastic excitations for seven model glass-forming liquids

Model	$T_{\rm o}$	$T_{\rm KT}^{\rm app}$	$T_{\rm KT}$
Poly-(12,0), ($\varepsilon = 0.2$)	0.25	0.38	0.27
Poly-(12,6), ($\varepsilon = 0.2$)	0.17	0.16	0.11
Poly-(18,0), ($\varepsilon = 0.0$)	1.10	2.00	1.40
Poly-(18,0), ($\varepsilon = 0.2$)	0.39	0.51	0.35
Poly-(10,6), ($\varepsilon = 0.1$)	0.17	0.35	0.24
Poly-(10,6), ($\varepsilon = 0.2$)	0.14	0.15	0.10
2D Kob–Andersen (KA) 65:35	1.00	1.34	0.94

The predicted $T_{\rm KT}$ is obtained by integrating the RG flow equation Eq. **7b** and **c**. For completeness, we also report the approximated transition temperatures $T_{\rm KT}^{\rm app}$, which assume that $\tilde{Y}^{\rm R} \approx \tilde{Y}^{\rm IS}$. For further numerical details, *SI Appendix*, section 5.4.

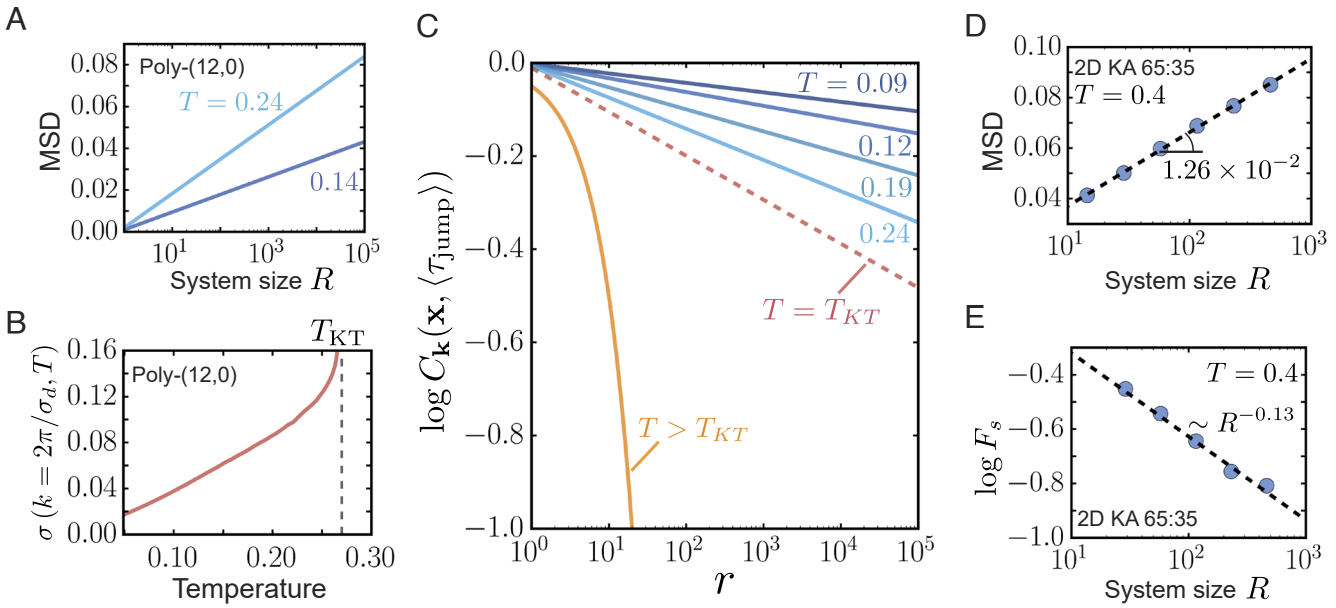

Fig. 4. Theoretical analysis and predictions from our theory applied to atomistic models of two-dimensional supercooled liquids. (*A*) Predicted mean squared displacement (MSD) vs. system size R for the Poly-(12,0) model at two different temperatures below $T_{\rm KT}$. In two dimensions, the elastic nature of the supercooled liquid in the glassy regime leads to a logarithmic system size dependence. (*B*) The power law exponent $\sigma(k, T)$ in Eq. **9b** vs. temperature for the Poly-(12,0) model for $k = 2\pi$. At low temperatures, it increases linearly as a result of $\gamma^{\rm R} \to \gamma^{\rm IS}$, while for $T \to T_{\rm KT}$, it increases abruptly because the material loses its rigidity. (*C*) Predicted spatial dependence of the correlation function $C_{\mathbf{k}}(\mathbf{x}, \langle\tau_{\rm jump}\rangle)$ for the Poly-(12,0) model glass former. (*D*) Fitted MSD vs. R data for the two-dimensional (2D) Kob–Andersen (KA) 65:35 model at $T = 0.4$ and $t = 100$ (47). (*E*) Fitted $F_S(k, t)$ vs. R data for the 2D KA 65:35 model at $T = 0.4$ (47), where $k = 2\pi/\sigma_{\rm d}$, with $\sigma_{\rm d} = 1$ and $t = 100$. Note that the scalings for the Poly-(12,0) model are predictions and are yet to be tested extensively through large-scale molecular simulations.

increasing system size at deep supercooled conditions due to Mermin–Wagner fluctuations alone.

In addition to finite-size effects, Mermin–Wagner fluctuations can also be probed spatially. To this end, we introduce an order parameter field $\rho_{\mathbf{k}}(\mathbf{x}, t) = e^{i\mathbf{k}\cdot\mathbf{u}(\mathbf{x}, t)}$ based on the displacement field $\mathbf{u}(\mathbf{x}, t)$, which is computed from the particle displacement $\mathbf{u}^{\alpha}(t)$. The spatial correlation function of $\rho_{\mathbf{k}}(\mathbf{x}, t)$ at $t \simeq \langle\tau_{\rm jump}\rangle$ is then

$$C_{\mathbf{k}}(\mathbf{x}, \langle\tau_{\rm jump}\rangle) := \left\langle \rho_{\mathbf{k}}\left(\mathbf{x}, \langle\tau_{\rm jump}\rangle\right) \rho_{-\mathbf{k}}\left(\mathbf{0}, 0\right)\right\rangle \qquad [10]$$

$$\simeq \left(\frac{|\mathbf{x}|}{R}\right)^{-\sigma(k,T)}, \qquad [11]$$

SI Appendix, section 5.5. Eq. **11** implies that spatial fluctuations of the order parameter field with respect to an initial inherent state exhibit power law correlations at intermediate timescales, thereby indicating quasi-long-range order reminiscent of 2D crystalline solids (34, 35). Such power law decay is in contrast to the exponential decay found in past studies of spatial correlations in supercooled liquids (16, 48), where structural order parameters were used to probe static correlations without reference to an initial inherent state. The power law exponent $\sigma(k, T)$, which also enters into the finite-size scaling in Eq. **9a**, increases with higher temperature, as seen in Fig. 4*B* for the predicted $\sigma(k, T)$ of the Poly-(12,0) model glass former. This results in a faster decay of correlations as $T \to T_{\rm KT}$ (Fig. 4*C*), with an expected exponential decay above $T_{\rm KT}$ corresponding to the fluid phase.

While Fig. 4 *A*–*C* show the predicted finite-size scalings for the Poly-(12,0) model glass former that are yet to be tested, we validate such scalings to available literature data. For instance, the 2D Kob–Andersen (KA) model (49) has been studied in large-scale molecular simulations (47), with data available for both the MSD and $F_s(k, t)$ at the same temperature ($T = 0.4$) for various system sizes. Fig. 4 *D* and *E* show the expected logarithmic and power law finite-size scalings of the MSD and $F_s(k, t)$, from Eqs. **8** and **9a**, respectively, for the 2D KA model when $t \approx 100$ and $k = 2\pi/\sigma_{\rm d}$. Note that these scalings also hold for a range of intermediate time scales less than the relaxation times. Furthermore, Eqs. **8** and **9b** predict that the exponents in both the MSD and $F_s(k, t)$ should be related to each other by a factor of $k^2/4$. Indeed, the fitted slope for $F_s(k, t)$ is $\sigma(k = 2\pi/\sigma_{\rm d}, T)/2 \approx 0.13$ and quantitatively agrees with the one obtained from the MSD, which is $(1.26 \times 10^{-2})k^2/4 \approx 0.124$, where $\sigma_{\rm d} = 1$ (47). These results constitute a first step in validating the theory in terms of the consequences for finite-size effects at the level of MSD and density autocorrelations. Further tests for temperature dependence of the exponents corresponding to the finite-size effects are left for future work.

The MSD and $F_s(k, t)$ can probe the emergence of solid-like nature and Mermin–Wagner fluctuations of 2D supercooled liquids. However, these results do not indicate the nature of the melting transition as they are tested deep in the supercooled regime. In what follows, we analyze the nature of the transition using experimental measurements obtained from a binary colloidal two-dimensional system confined to a water–air interface (50).

Connection to Experiments in Confined Colloids. Unlike a conventional melting transition, the IS melting is not a true equilibrium phenomenon since it is mediated dynamically by elastic excitations at short-intermediate timescales. Its signatures may manifest just below the onset temperature $T_{\rm o}$ if we measure the elastic moduli from displacement fluctuations at timescales $t \simeq \langle\tau_{\rm jump}\rangle \ll \tau_{\rm eq}(T)$ in the long-wavelength limit $k \to 0$.

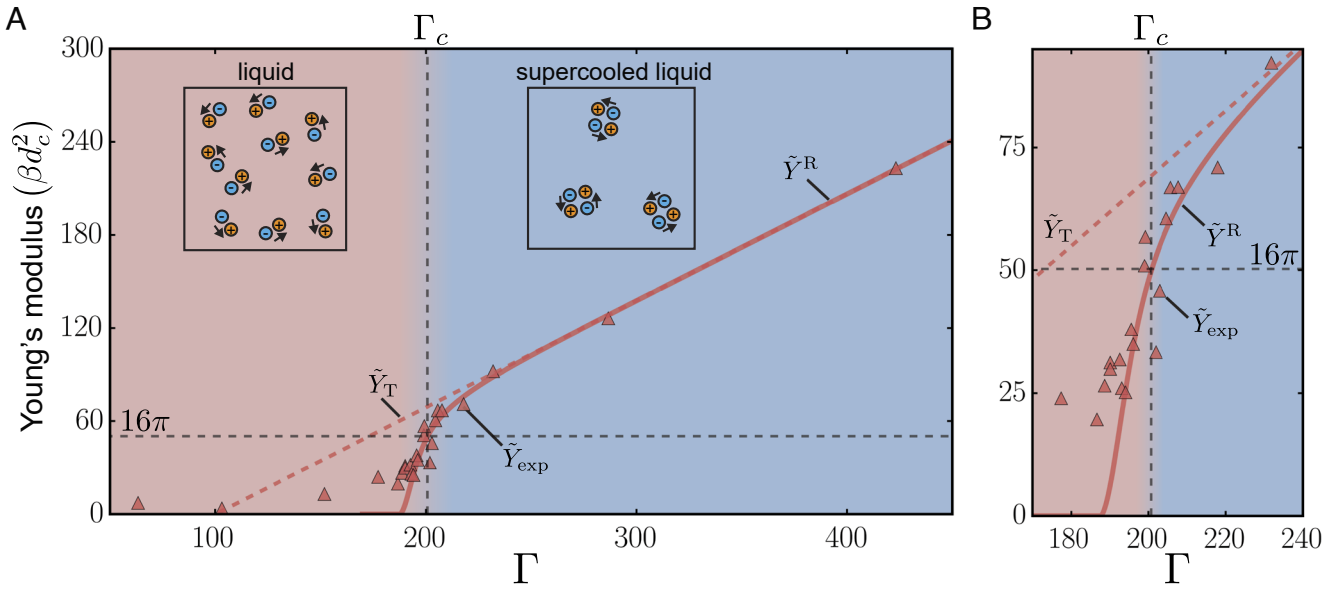

Fig. 5. (*A*) Experimentally measured normalized Young's $\tilde{Y}_{exp} = \beta d_c^2 Y_{exp}$ (red △) modulus for a binary colloidal system confined to a water–air interface (50). The theoretically predicted renormalized Young's $\tilde{Y}^R$ modulus is shown in continuous lines, while we show with dashed line the bare Young's modulus $\tilde{Y}_T$. The vertical and horizontal dashed gray lines correspond to the universal value of 16π for Young's modulus and the critical value of Γ_c predicted by the RG calculation, respectively. (*B*) Magnified view of Young's modulus near the transition point indicating the softening of the system due to bound dipole excitations. Our RG analysis predicts vanishing moduli at $\Gamma_c\,(\ell = \ln(R/\sigma_d)) \simeq 200$, close to the experimentally suggested value of $\Gamma_c^{exp} = 195 \pm 5$. For infinite system sizes, $\tilde{Y}^R$ vanishes discontinuously at $\Gamma_c\,(\ell \to \infty) \simeq 203$, and the normalized Young's modulus attains the universal value of 16π analogous to the KTHNY scenario (34–39). The value of Γ_c allows us to distinguish the liquid (red area) from the supercooled liquid (blue area) regimes. The *Insets* provide illustrations of the elastic excitations that would be present in these distinct regimes corresponding to free dipoles and bound dipole-pairs, respectively.

From these measurements, we expect that Young's modulus reaches 16π before it vanishes to zero in a discontinuous manner at $T = T_o$. When finite-size effects are present, the discontinuity would turn into a smooth but steep transition.

Klix et al. (50–52) have performed such measurements in experiments that involve a binary colloidal system confined to a water–air interface, a setup specially designed for probing 2D physics (53). Note that the single-component version of this system has been originally used to validate the KTHNY theory of 2D crystal melting (54), motivating the design of the binary version to probe 2D glassy dynamics (55). In their experimental setup, the particles are paramagnetic and interact repulsively upon tuning the strength of the externally applied magnetic field H. The interaction strength is controlled with respect to thermal energy through a single dimensionless group Γ that scales as $\Gamma \sim \beta H^2$ (50, 52). In particular, by increasing H, they are able to access the supercooled regime and probe the corresponding elastic behavior at intermediate timescales. The shear G_{exp} and bulk B_{exp} moduli are then computed through a set of fluctuation formulas (46) (*SI Appendix*, section 5.6) that read as

$$\lim_{k\to 0} \frac{1}{k^2 \left\langle |\hat{\mathbf{u}}_{\parallel}(\mathbf{k})|^2 \right\rangle} = \beta (G_{exp} + B_{exp}) \sigma_d^2, \qquad [12]$$

$$\lim_{k\to 0} \frac{1}{k^2 \left\langle |\hat{\mathbf{u}}_{\perp}(\mathbf{k})|^2 \right\rangle} = \beta G_{exp} \sigma_d^2, \qquad [13]$$

where σ_d is the mean interparticle distance, $\hat{\mathbf{u}}(\mathbf{k})$ is the Fourier-transformed displacement fields obtained via microscopy, $\hat{\mathbf{u}}_{\parallel}(\mathbf{k}) = \hat{\mathbf{k}} \cdot \hat{\mathbf{u}}(\mathbf{k})$ and $\hat{\mathbf{u}}_{\perp}(\mathbf{k}) = \hat{\mathbf{u}}(\mathbf{k}) - \hat{\mathbf{u}}_{\parallel}(\mathbf{k})$ are the longitudinal and transverse displacement, respectively, and $\hat{\mathbf{k}} = \mathbf{k}/k$. Klix et al. (50–52) find that G_{exp} decreases abruptly to values close to zero at approximately $\Gamma_c^{exp} = 195 \pm 5$ (*SI Appendix*, Fig. S.26) and observe that the dimensionless Young's modulus $\beta Y_{exp} \sigma_d^2$ also reaches 16π (*SI Appendix*, Fig. S.27). Thus, the transition point appears to distinguish the high-temperature (low Γ) from the supercooled regime (high Γ) and signal the loss of rigidity at intermediate timescales.

The experimental observations on the vanishing moduli at a specific 'inverse effective temperature' Γ_c^{exp} suggest the relevance of our theory to explain the emergence of rigidity at supercooled conditions ($\Gamma > \Gamma_c^{exp}$) and finite timescales. We test this hypothesis by applying the RG equations (Eq. **7a** and **b**) to the confined binary colloidal system, a task that requires the bare Young's modulus and fugacity as input. For the bare Young's modulus Y_T, we use the experimentally observed values in the supercooled regime ($\Gamma \geq 232$), where softening due to excitations is assumed negligible, and extrapolate its trend to the low-Γ regime (*SI Appendix*, section 5.6). Estimating the bare fugacity $\tilde{y}$ involves the dipole magnitude d_c, which requires the IS radial distribution function (RDF) as input. Since the IS RDF is not available from the experiments, we instead use the RDF of the big particles $g_{bb}(r)$ and small particles $g_{ss}(r)$ obtained at $\Gamma = 556$ (56, 57) as proxies for the IS local structure. Assuming that there are two kinds of excitations breaking a bond in a pair of small and large particles, respectively, we estimate d_c, and thereby $\tilde{y}$, following an application of the mixture rule similar to DF theory (4) (*SI Appendix*, section 5.6).

Fig. 5 shows the dimensionless Young's modulus from experiments $\tilde{Y}_{exp}$, the extrapolated bare values $\tilde{Y}_T$, and the predicted $\tilde{Y}^R$ based on the RG equations (Eq. **7a** and **b**). Here, we see two mechanisms responsible for the softening of the system that leads to the experimentally observed transition. The first softening mechanism is due to vibrational fluctuations, as indicated by the linearity and nonzero intercept of $\tilde{Y}_T$ (55, 58); *SI*

Appendix, section 5.6. Approaching the transition, the predicted $\tilde{Y}^{\mathrm{R}}$ deviates from this linear behavior, indicating the second softening mechanism that results due to the existence of bound dipole elastic excitations. Furthermore, $\tilde{Y}^{\mathrm{R}}$ follows closely the experimental values $\tilde{Y}_{\mathrm{exp}}$, and the predicted transition point $\Gamma_{\mathrm{c}} \simeq 200$ also agrees with the experimentally suggested value $\Gamma_{\mathrm{c}}^{\mathrm{exp}} = 195 \pm 5$. Taken together, these results highlight the unbinding of bound elastic dipolar excitations as the leading mechanism for the loss of rigidity. It is also notable that our RG calculations capture the continuous but abrupt decrease of $\tilde{Y}^{\mathrm{R}}$ instead of the discontinuous behavior previously shown in Fig. 3*B*). This behavior is caused by finite-size effects, which we account for by setting the upper limit of the integration of the RG equations to $\ell = \log(R/\sigma_{\mathrm{d}})$, where $R = 20.5\sigma_{\mathrm{d}}$ is the experimental system size (50, 52).

Conclusions and Discussion

In summary, we construct a theory for the onset temperature T_{o} of glassy dynamics in two dimensions (2D), starting from the isoconfigurational ensemble (40) as a basis for the statistical mechanics of excitations in supercooled liquids. The resulting framework allows us to derive the Arrhenius form for the rate/concentration of excitations, $c_{\mathrm{eq}}(T) \sim e^{-\beta \tilde{E}_{\mathrm{c}}}$, which is empirically found in the DF theory when performing rate calculations from molecular simulations (17, 19). To understand the onset of glassy dynamics, excitations are represented as interacting geometric dipoles, a description unique to the 2D nature of the liquids. Analogous to the KTHNY theory (34–39), T_{o} can be described as the temperature where the binding-unbinding transition of dipolar elastic excitations, as well as melting of inherent states, occurs. The predicted T_{o} is in reasonable agreement with those observed across seven different model glass formers (Table 1). Additionally, the proposed scenario of the binding-unbinding transition of dipolar elastic excitations quantitatively describes experimental observations on the vanishing elastic moduli in two-dimensional binary colloidal glass formers (50). The theory also enables studies on displacement and density correlations, where the predicted finite-size scalings are consistent with recent observations of Mermin–Wagner fluctuations from simulations and experiments in 2D glass formers (11–15).

Given the reasonable agreement between the theoretical predictions for T_{o} and the renormalized elastic moduli with molecular simulations and experiments (Table 1 and Fig. 5), the observed transition can also be interpreted as the onset of glassy dynamics. Since our theory governs the nature of hopping processes or IS jumps, we find that below $T_{\mathrm{KT}} \approx T_{\mathrm{o}}$ localized mobile regions are intimately linked to bound dipole-pair excitations that are sparsely distributed across the elastic medium (19, 28) and soften the underlying solid. Additionally, within the supercooled regime, localized excitation events drive the relaxation of the material, which occurs by cascading excitations that appear in a hierarchical manner, i.e., dynamical facilitation (17, 18). Once the temperature is increased above T_{o}, the liquid is able to relax upon the first IS jump through the formation of free dipolar excitations, allowing the system to behave as a fluid. Thus, T_{o} signals a change in the relaxation mechanism between the supercooled and high-temperature regimes; Fig. 5, *Insets*.

In the proposed theory, the origin of T_{o} lies within the isoconfigurational ensemble, and thus the inherent-state melting transition is a hidden transition that may not be observable directly from the liquid thermodynamic properties. Furthermore, analyzing this transition may be difficult upon noting the required separation of timescales Eq. **1**, which may limit the range of applicability of our theory near T_{o}. However, the reasonable agreement between the predicted and observed T_{o}, as well as the RG calculation with experimental observations of a 2D binary colloidal system (Fig. 5), suggests that the theory is useful in interpreting the emergence of glassy dynamics at T_{o} as the onset of inherent-state stability against excitation fluctuations. This understanding of inherent-state stability should be contrasted to the one obtained from mean-field approaches (23, 25). These theories predict another transition temperature, namely the dynamic transition temperature T_{d}, where the system loses its rigidity due to fluctuations that are independent from any type of activated processes, including excitation events. The exact nature of the transition in mean-field approaches remains an open question (25) with some analyses predicting a discontinuous transition (24, 59), e.g., the shear modulus is described as $G(T) = G(T_{\mathrm{d}}) + C\,(T_{\mathrm{d}} - T)^{1/2}$ for $T < T_{\mathrm{d}}$, while other ones (60, 61) based on the replica theory (62) predict a continuous transition instead. Nevertheless, the onset temperature T_{o} is understood to be distinct from T_{d} (25) since $\tau_{\mathrm{eq}}(T)$ has non-Arrhenius behavior at $T_{\mathrm{d}} < T < T_{\mathrm{o}}$ (23, 24). Thus, while our theory and the mean-field approaches share a similar premise, the present proposal constitutes an alternative perspective to understand the emergence of rigidity and relaxation of supercooled liquids, with elastic dipole-pair excitations as the underlying mechanism.

Further tests need to be performed through simulations using the isoconfigurational ensemble (40) and in particular on the temperature dependence of the MSD and spatial correlations in density fluctuations. Experiments through (quasi-)2D colloidal systems (13, 14, 50) also provide an additional platform to test the theory through finite-size effects. Last, even though our work sheds light on the onset temperature in 2D, the nature of the onset temperature in three dimensions (3D) remains an open question. The corresponding 3D theory may require an extension of the elastic dipolar excitations to physical objects similar to dislocation loops (63, 64). Consequently, we hypothesize that the corresponding theory in 3D also involves inherent-state melting that may now be mediated by loop excitations. We leave the possibility of such a theory for future work.

Materials and Methods

The derivation steps of the theory and the relevant computational methods in this work are detailed in *SI Appendix*. *SI Appendix*, section 1 describes the statistical mechanics framework of excitations, leading to the final grand canonical partition function in Eq. **3a** and **b**. *SI Appendix*, section 2 reviews the geometric charges framework (29, 30) for modeling elastic excitations proposed in this work. *SI Appendix*, sections 3 and 5.1–5.3 contain the energy–entropy arguments and the renormalization group (RG) procedure, respectively, that lead toward the calculation of onset temperature T_{o}. *SI Appendix*, section 5.4 provides details on computer simulations of the continuous polydisperse glass formers (65) used in this work. These computational details include the molecular dynamics and Monte Carlo simulations as well as the procedures to generate the data for the relaxation time (i.e., Fig. 1*A*), mean squared displacement (i.e., Fig. 1*B*), the bare and renormalized inherent-state (IS) elastic constants (i.e., Fig. 3*B*), as well as the RG calculations (i.e., Fig. 3*A*) for predicting the onset temperature (i.e., Table 1). *SI Appendix*, section 5.5 includes the derivations for the Mermin–Wagner finite-size scalings and power laws presented in Fig. 5 *C*–*E* and Eqs. **8**–**11**. Last, *SI Appendix*, section 5.6 includes details on how the RG equations Eq. **7a** and **b** are applied to predict the elastic moduli of an experimental colloidal

system involving paramagnetic particles confined to a water–air interface (50, 52).

Data, Materials, and Software Availability. All study data are included in the article and/or *SI Appendix*. Data generating the figures are also deposited in our GitHub repo, https://github.com/mandadapu-group/pnas-inherent-melting (66).

ACKNOWLEDGMENTS. We acknowledge Cory Hargus for insightful comments on the manuscript. D.F. (dfrag) acknowledges support from the Miller Institute for Basic Research in Science at University of California, Berkeley. M.R.H. and K.K.M. were entirely supported by the Director, Office of Science, Office of Basic Energy Sciences, of the US Department of Energy under Contract No. DEAC02-05CH1123.

Author affiliations: [a]Department of Chemical & Biomolecular Engineering, University of California, Berkeley, CA 94720; and [b]Chemical Sciences Division, Lawrence Berkeley National Laboratory, Berkeley, CA 94720

Author contributions: D.F., M.R.H., and K.K.M. designed research; performed research; contributed new reagents/analytic tools; analyzed data; and wrote the paper.

1. C. A. Angell, K. L. Ngai, G. B. McKenna, P. F. McMillan, S. W. Martin, Relaxation in glassforming liquids and amorphous solids. *J. Appl. Phys.* **88**, 3113–3157 (2000).
2. A. Cavagna, Supercooled liquids for pedestrians. *Phys. Rep.* **476**, 51–124 (2009).
3. Y. S. Elmatad, D. Chandler, J. P. Garrahan, Corresponding states of structural glass formers. *J. Phys. Chem. B* **113**, 5563–5567 (2009).
4. S. Katira, J. P. Garrahan, K. K. Mandadapu, Theory for glassy behavior of supercooled liquid mixtures. *Phys. Rev. Lett.* **123**, 100602 (2019).
5. L. Berthier, G. Biroli, Theoretical perspective on the glass transition and amorphous materials. *Rev. Mod. Phys.* **83**, 587 (2011).
6. R. Zwanzig, *Nonequilibrium Statistical Mechanics* (Oxford University Press, 2001).
7. G. H. Vineyard, Scattering of slow neutrons by a liquid. *Phys. Rev.* **110**, 999 (1958).
8. T. B. Schrøder, J. C. Dyre, Solid-like mean-square displacement in glass-forming liquids. *J. Chem. Phys.* **152**, 141101 (2020).
9. N. D. Mermin, H. Wagner, Absence of ferromagnetism or antiferromagnetism in one- or two-dimensional isotropic Heisenberg models. *Phys. Rev. Lett.* **17**, 1133–1136 (1966).
10. N. D. Mermin, Crystalline order in two dimensions. *Phys. Rev.* **176**, 250–254 (1968).
11. E. Flenner, G. Szamel, Fundamental differences between glassy dynamics in two and three dimensions. *Nat. Comm.* **6**, 1–6 (2015).
12. H. Shiba, Y. Yamada, T. Kawasaki, K. Kim, Unveiling dimensionality dependence of glassy dynamics: 2D infinite fluctuation eclipses inherent structural relaxation. *Phys. Rev. Lett.* **117** (2016).
13. B. Illing *et al*., Mermin-Wagner fluctuations in 2D amorphous solids. *Proc. Natl. Acad. Sci. U.S.A.* **114**, 1856–1861 (2017).
14. S. Vivek, C. P. Kelleher, P. M. Chaikin, E. R. Weeks, Long-wavelength fluctuations and the glass transition in two dimensions and three dimensions. *Proc. Natl. Acad. Sci. U.S.A.* **114**, 1850–1855 (2017).
15. G. Tarjus, Glass transitions may be similar in two and three dimensions, after all. *Proc. Natl. Acad. Sci. U.S.A.* **114**, 2440–2442 (2017).
16. L. Berthier, G. Biroli, J. P. Bouchaud, L. Cipelletti, W. van Saarloos, *Dynamical Heterogeneities in Glasses, Colloids, and Granular Media* (OUP Oxford, 2011), vol. 150.
17. A. S. Keys, L. O. Hedges, J. P. Garrahan, S. C. Glotzer, D. Chandler, Excitations are localized and relaxation is hierarchical in glass-forming liquids. *Phys. Rev. X* **1**, 021013 (2011).
18. B. Guiselin, C. Scalliet, L. Berthier, Microscopic origin of excess wings in relaxation spectra of supercooled liquids. *Nat. Phys.* **18**, 468–472 (2022).
19. M. R. Hasyim, K. K. Mandadapu, A theory of localized excitations in supercooled liquids. *J. Chem. Phys.* **155**, 044504 (2021).
20. F. H. Stillinger, T. A. Weber, Hidden structure in liquids. *Phys. Rev. A* **25**, 978 (1982).
21. D. Chandler, J. P. Garrahan, Dynamics on the way to forming glass: Bubbles in space-time. *Ann. Rev. Phys. Chem.* **61**, 191–217 (2010).
22. J. P. Garrahan, D. Chandler, Geometrical explanation and scaling of dynamical heterogeneities in glass forming systems. *Phys. Rev. Lett.* **89**, 035704 (2002).
23. D. R. Reichman, P. Charbonneau, Mode-coupling theory. *J. Stat. Mech.: Theory Exp.* **2005**, P05013 (2005).
24. W. Götze, *Complex Dynamics of Glass-Forming Liquids: A Mode-Coupling Theory* (Oxford University Press on Demand, 2009), vol. 143.
25. G. Biroli, J. P. Bouchaud, "The random first-order transition theory of glasses: A critical assessment" in *Structural Glasses and Supercooled Liquids: Theory, Experiment, and Applications* (Wiley New York, 2012), pp. 31–113.
26. J. C. Dyre, Colloquium: The glass transition and elastic models of glass-forming liquids. *Rev. Mod. Phys.* **78**, 953–972 (2006).
27. T. B. Schrøder, S. Sastry, J. C. Dyre, S. C. Glotzer, Crossover to potential energy landscape dominated dynamics in a model glass-forming liquid. *J. Chem. Phys.* **112**, 9834–9840 (2000).
28. R. N. Chacko *et al*., Elastoplasticity mediates dynamical heterogeneity below the mode coupling temperature. *Phys. Rev. Lett.* **127**, 048002 (2021).
29. M. Moshe, I. Levin, H. Aharoni, R. Kupferman, E. Sharon, Geometry and mechanics of two-dimensional defects in amorphous materials. *Proc. Natl. Acad. Sci. U.S.A.* **112**, 10873–10878 (2015).
30. M. Moshe, E. Sharon, R. Kupferman, Elastic interactions between two-dimensional geometric defects. *Phys. Rev. E* **92**, 062403 (2015).
31. E. Lerner, E. Bouchbinder, Low-energy quasilocalized excitations in structural glasses. *J. Chem. Phys.* **155**, 200901 (2021).
32. D. Khomenko, C. Scalliet, L. Berthier, D. R. Reichman, F. Zamponi, Depletion of two-level systems in ultrastable computer-generated glasses. *Phys. Rev. Lett.* **124**, 225901 (2020).
33. W. Ji, T. W. de Geus, E. Agoritsas, M. Wyart, Mean-field description for the architecture of low-energy excitations in glasses. *Phys. Rev. E* **105**, 044601 (2022).
34. J. M. Kosterlitz, D. J. Thouless, Long range order and metastability in two dimensional solids and superfluids. Application of dislocation theory. *J. Phys. C: Solid State Phys.* **5**, L124 (1972).
35. J. M. Kosterlitz, D. J. Thouless, Ordering, metastability and phase transitions in two-dimensional systems. *J. Phys. C: Solid State Phys.* **6**, 1181 (1973).
36. B. Halperin, D. R. Nelson, Theory of two-dimensional melting. *Phys. Rev. Lett.* **41**, 121 (1978).
37. D. R. Nelson, Study of melting in two dimensions. *Phys. Rev. B* **18**, 2318 (1978).
38. D. R. Nelson, B. Halperin, Dislocation-mediated melting in two dimensions. *Phys. Rev. B* **19**, 2457 (1979).
39. A. Young, Melting and the vector Coulomb gas in two dimensions. *Phys. Rev. B* **19**, 1855 (1979).
40. A. Widmer-Cooper, P. Harrowell, H. Fynewever, How reproducible are dynamic heterogeneities in a supercooled liquid? *Phys. Rev. Lett.* **93**, 135701 (2004).
41. D. Chandler, Statistical mechanics of isomerization dynamics in liquids and the transition state approximation. *J. Chem. Phys.* **68**, 2959–2970 (1978).
42. B. Peters, *Reaction Rate Theory and Rare Events* (Elsevier, 2017).
43. J. P. Garrahan, D. Chandler, Coarse-grained microscopic model of glass formers. *Proc. Natl. Acad. Sci. U.S.A.* **100**, 9710–4 (2003).
44. F. Ritort, P. Sollich, Glassy dynamics of kinetically constrained models. *Adv. Phys.* **52**, 219–342 (2003).
45. N. Goldenfeld, *Lectures on Phase Transitions and the Renormalization Group* (CRC Press, 2018).
46. M. Kardar, *Statistical Physics of Fields* (Cambridge University Press, 2007).
47. H. Shiba, T. Kawasaki, K. Kim, Local density fluctuation governs the divergence of viscosity underlying elastic and hydrodynamic anomalies in a 2D glass-forming liquid. *Phys. Rev. Lett.* **123**, 265501 (2019).
48. J. E. Hallett, F. Turci, C. P. Royall, Local structure in deeply supercooled liquids exhibits growing lengthscales and dynamical correlations. *Nat. Comm.* **9**, 1–10 (2018).
49. W. Kob, H. C. Andersen, Testing mode-coupling theory for a supercooled binary Lennard-Jones mixture i: The van Hove correlation function. *Phys. Rev. E* **51**, 4626 (1995).
50. C. L. Klix, G. Maret, P. Keim, Discontinuous shear modulus determines the glass transition temperature. *Phys. Rev. X* **5**, 041033 (2015).
51. C. L. Klix *et al*., Glass elasticity from particle trajectories. *Phys. Rev. Lett.* **109** (2012).
52. C. L. Klix, "Spectroscopy of displacements in a two-dimensional colloidal glass former," PhD, thesis, Universität Konstanz (2014).
53. F. Ebert, P. Dillmann, G. Maret, P. Keim, The experimental realization of a two-dimensional colloidal model system. *Rev. Sci. Instrum.* **80** (2009).
54. H. H. von Grünberg, P. Keim, K. Zahn, G. Maret, Elastic behavior of a two-dimensional crystal near melting. *Phys. Rev. Lett.* **93**, 255703 (2004).
55. H. König, R. Hund, K. Zahn, G. Maret, Experimental realization of a model glass former in 2D. *Eur. Phys. J. E* **18**, 287–293 (2005).
56. F. Ebert, P. Keim, G. Maret, Local crystalline order in a 2D colloidal glass former. *Eur. Phys. J. E* **26**, 161–168 (2008).
57. F. Ebert, "Dynamics and structure of a colloidal glass former in two dimensions," PhD, thesis, Universität Konstanz (2008).
58. J. H. Weiner, *Statistical Mechanics of Elasticity* (Courier Corporation, 2012).
59. T. Kirkpatrick, P. Wolynes, Connections between some kinetic and equilibrium theories of the glass transition. *Phys. Rev. A* **35**, 3072 (1987).
60. H. Yoshino, M. Mézard, Emergence of rigidity at the structural glass transition: A first-principles computation. *Phys. Rev. Lett.* **105**, 015504 (2010).
61. H. Yoshino, Replica theory of the rigidity of structural glasses. *J. Chem. Phys.* **136**, 214108 (2012).
62. M. Mézard, G. Parisi, A first-principle computation of the thermodynamics of glasses. *J. Chem. Phys.* **111**, 1076–1095 (1999).
63. R. de Wit, The continuum theory of stationary dislocations. *Solid State Phys.* **10**, 249–292 (1960).
64. H. Kleinert, *Gauge Fields in Condensed Matter* (World Scientific, 1989), vol. 2.
65. A. Ninarello, L. Berthier, D. Coslovich, Models and algorithms for the next generation of glass transition studies. *Phys. Rev. X* **7**, 021039 (2017).
66. D. Fraggedakis, M.R. Hasyim, K.K. Mandadapu, Data for Inherent-state melting and the onset of glassy dynamics in two-dimensional supercooled liquids. https://github.com/mandadapu-group/pnas-inherent-melting. Deposited 16 March 2023.